Journal of Materials Chemistry C

ROYAL SOCIETY OF CHEMISTRY

PAPER

View Article Online
View Journal | View Issue

Cite this: J. Mater. Chem. C, 2022, 10, 2742

Finely modulated asymmetric nonfullerene acceptors enabling simultaneously improved voltage and current for efficient organic solar cells†

Huanhuan Gao,[ab] Xiangjian Wan,[b] Ziyi Xuan,[c] Wei Ma,*[c] Jingming Xin,[c] Chenxi Li[b] and Yongsheng Chen*[b]

Received 12th August 2021,
Accepted 19th October 2021

DOI: 10.1039/d1tc03793e

rsc.li/materials-c

It is a great challenge to simultaneously improve the short-circuit current density (J_{sc}) and open-circuit voltage (V_{oc}) of organic solar cells (OSCs) owing to the trade-off effect between the two photovoltaic parameters. Delicate chemical structure modulation of the active layer materials is always one of the effective strategies to address this issue. In this work, following a simple and efficient strategy through fine-tuning the molecular configuration in combination with the side chain modulation to address the issue, three non-fullerene acceptors (NFAs), **5T-2C8-IN**, **5T-2C8-Cl** and **5T-2C8-2Cl** with a five-thiophene (5T) fused asymmetric molecular backbone and octyl side chains at the terminal position of the molecular backbone, have been designed and synthesized. Among them, the **5T-2C8-2Cl** based photovoltaic device showed a power conversion efficiency (PCE) of 13.02% with a simultaneously improved V_{oc} of 0.802 V and a J_{sc} of 24.97 mA cm^{-2} compared with the device of the control acceptor **6T-2C8-2Cl** with a PCE of 12.43%, a V_{oc} of 0.785 V and a J_{sc} of 24.40 mA cm^{-2}.

1. Introduction

Organic solar cells (OSCs) have witnessed a great progress in the past decade.[1–4] The state-of-the-art OSCs have achieved impressive efficiencies of over 18% thanks to the invention of new active layer materials especially non fullerene acceptors (NFAs) and device engineering.[5–10] NFAs with broad absorptions up to the near-infrared range have proved to be an effective strategy to harvest more solar irradiation and obtain enhanced J_{sc} values. However, the decrease of the bandgaps of acceptor materials inevitably leads to a concomitant reduction in the V_{oc} value.[11] Thus, the trade-off issue between the V_{oc} and J_{sc} limits the overall PCE values of OSC devices. Obtaining balanced and best values for V_{oc} and J_{sc} has become a great challenge for active material design and device optimization. Finely tuning the absorption ranges and energy level alignments of the active layers have been regarded as the effective way to address the above trade-off issue of V_{oc} and J_{sc}.[12–14] In fact, many efforts have been devoted to designing active layer materials, especially the donor–acceptor–donor (A–D–A) type NFAs from multiple perspectives to encounter this issue. Generally, A–D–A NFAs have a ladder-type electron-rich conjugation skeleton with two electron-deficient end groups.[15–17] In order to precisely regulate NFAs' properties, fine-tuning the chemical structures *via* modification of the central core,[18–23] the side chains[24–27] or end groups[28–30] has attracted extensive attention and led to great success in the past decade.[31–35]

In our previous work, we have developed a strategy to improve V_{oc} and J_{sc} synergistically by a simple and effective side chain modulation on the six thiophene (6T) fused symmetric backbone of an A–D–A type acceptor.[12] Recently, asymmetric NFAs have been proposed as a simple but effective strategy for precise regulation of molecular structures.[36–39] It has been demonstrated that asymmetric structures could induce a larger dipole moment and an enhanced intramolecular structure charge transfer, thus leading to enhanced intermolecular charge transfer (ICT) and stronger intermolecular binding energy compared with the symmetric ones.[40,41] In this work, based on our previous work of side chain modulation at the terminal position of the molecular backbone and the advantages of asymmetric acceptors, we have designed and synthesized three asymmetric NFAs, **5T-2C8-IN**, **5T-2C8-Cl** and **5T-2C8-2Cl** with 5T fused asymmetric skeletons and octyl side

[a] Xi'an Key Laboratory of High Performance Oil and Gas Field Materials, School of Materials Science and Engineering, Xian Shiyou University, Shaanxi, Xi'an 710065, China
[b] Key Laboratory of Functional Polymer Materials, College of Chemistry, Renewable Energy Conversion and Storage Center (RECAST), Nankai University, Tianjin 300071, China. E-mail: yschen99@nankai.edu.cn
[c] State Key Laboratory for Mechanical Behavior of Materials, Xi'an Jiaotong University, Xi'an 710049, China. E-mail: msewma@mail.xjtu.edu.cn

† Electronic supplementary information (ESI) available. See DOI: 10.1039/d1tc03793e

chains at the terminal position of the molecular backbone. Among them, **5T-2C8-2Cl** showed redshifted absorption with absorption edge up to 960 nm. Compared with the control molecule **6T-2C8-2Cl** with a 6T fused symmetric molecular backbone,[12] **5T-2C8-2Cl** demonstrated an up-shifted LUMO energy level but a slightly red-shifted absorption edge. The OSC based on PM6:**5T-2C8-2Cl** achieved a higher PCE of 13.02% with an enhanced V_{oc} of 0.802 V and an improved J_{sc} of 24.97 mA cm^{-2} compared with the PM6:**6T-2C8-2Cl** based device with a PCE of 12.43%, a V_{oc} of 0.785 V and a J_{sc} of 24.40 mA cm^{-2}. These results demonstrate that careful molecular modulation from the perspective of an asymmetric molecular backbone as well as the side chain modulation is an effective strategy to address the challenge of the trade-off issue between V_{oc} and J_{sc}.

2. Results and discussion

2.1. Synthesis and characterization

The synthetic route of the three asymmetric acceptors **5T-2C8-IN**, **5T-2C8-Cl** and **5T-2C8-2Cl** is depicted in Scheme 1. The control symmetric acceptor **6T-2C8-2Cl** was prepared following our reported method.[12] The detailed synthesis procedures and characterization data of the three asymmetric acceptors are summarized in the ESI.† As shown in Scheme 1, the intermediate **3** was obtained with two step Stille coupling reactions with **a** and **b**. Then, the intermediate **5T-2C8** was synthesized *via* the intramolecular cyclization reaction from compound **3**. Subsequently, the intermediate **5T-2C8** was reacted with the Vilsmeier–Haack reagent to afford dialdehyde **5T-2C8-2CHO**. Finally, the target asymmetric acceptors were obtained through Knoevenagel condensation of **5T-2C8-2CHO** with different end groups. The intermediates and the target molecules are well characterized by ^{1}H NMR, ^{13}C NMR, and HR-MS, the details of which are presented in the ESI.†

2.2. Photophysical and electrochemical properties

The ultraviolet-visible absorption spectra of **5T-2C8-IN**, **5T-2C8-Cl**, **5T-2C8-2Cl** and **6T-2C8-2Cl** both in diluted solution and thin films were studied to investigate the influence of the backbone structure and the number of chlorine atoms on the optical properties. As shown in Fig. S1 (ESI†), in diluted chloroform solution, the maximum absorption peaks of **5T-2C8-IN**, **5T-2C8-Cl** and **5T-2C8-2Cl** were located at 770 (ε = 2.44 × 10^5 M^{-1} cm^{-1}), 785 (ε = 2.61 × 10^5 M^{-1} cm^{-1}), and 796 (ε = 2.64 × 10^5 M^{-1} cm^{-1}), respectively. In contrast, **6T-2C8-2Cl** showed redshifted absorption with maximum absorption peaks at 809 nm (ε = 2.41 × 10^5 M^{-1} cm^{-1}) owing to its enlarged conjugation length. In the solid film state, these three 5T acceptors all showed clear red-shifted absorptions compared with their absorptions in solution, demonstrating strong intermolecular interactions (Fig. 1). Surprisingly, **5T-2C8-2Cl** demonstrated a red-shifted absorption peak (871 nm) in comparison with the control molecule **6T-2C8-2Cl** (860 nm). Besides, a density functional theoretical (DFT) calculation based on the B3LYP/6-31G(d) level by Gaussian 16 (Fig. S3, ESI†) has been performed to further investigate the performance variation. To simplify the calculation process, the long alkyl chains were replaced with methyl groups. It can be seen from the calculation results that the four acceptors all exhibit

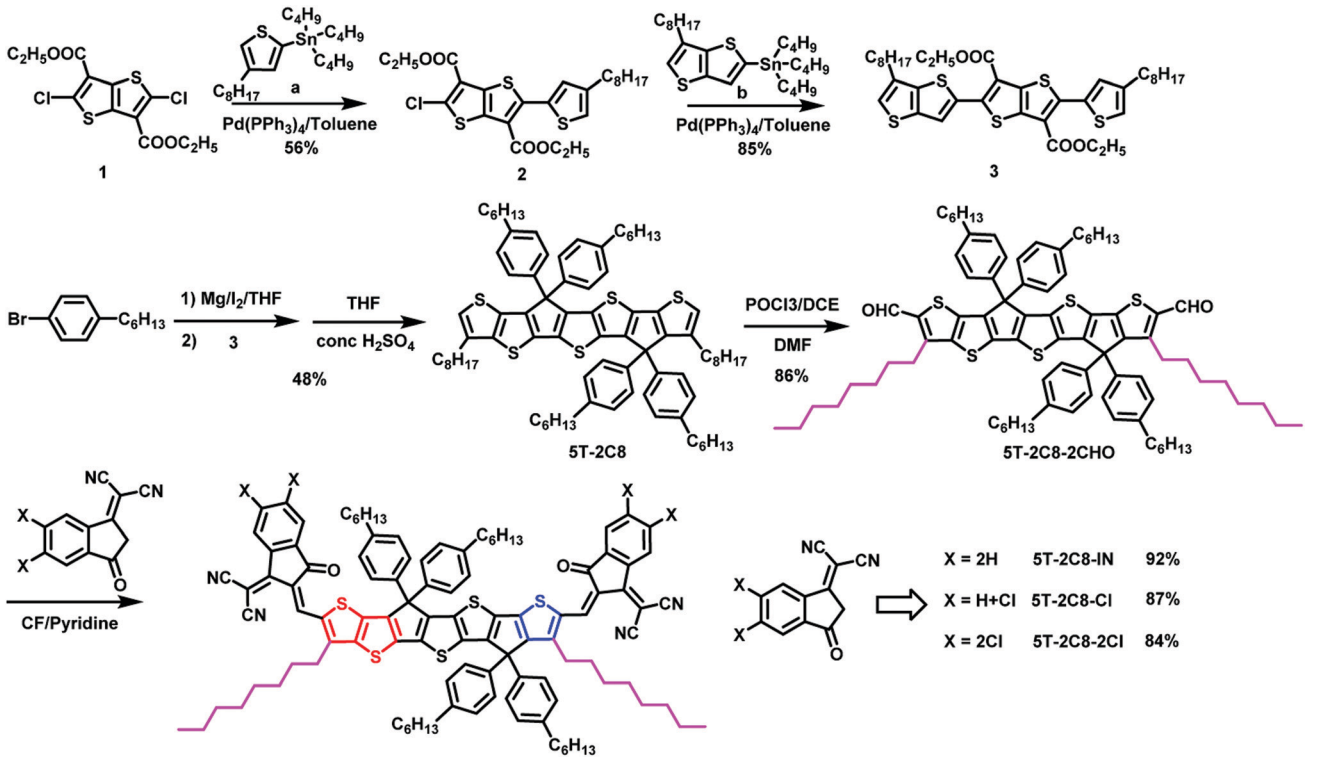

Scheme 1 The synthetic routes of **5T-2C8-IN**, **5T-2C8-Cl** and **5T-2C8-2Cl**.

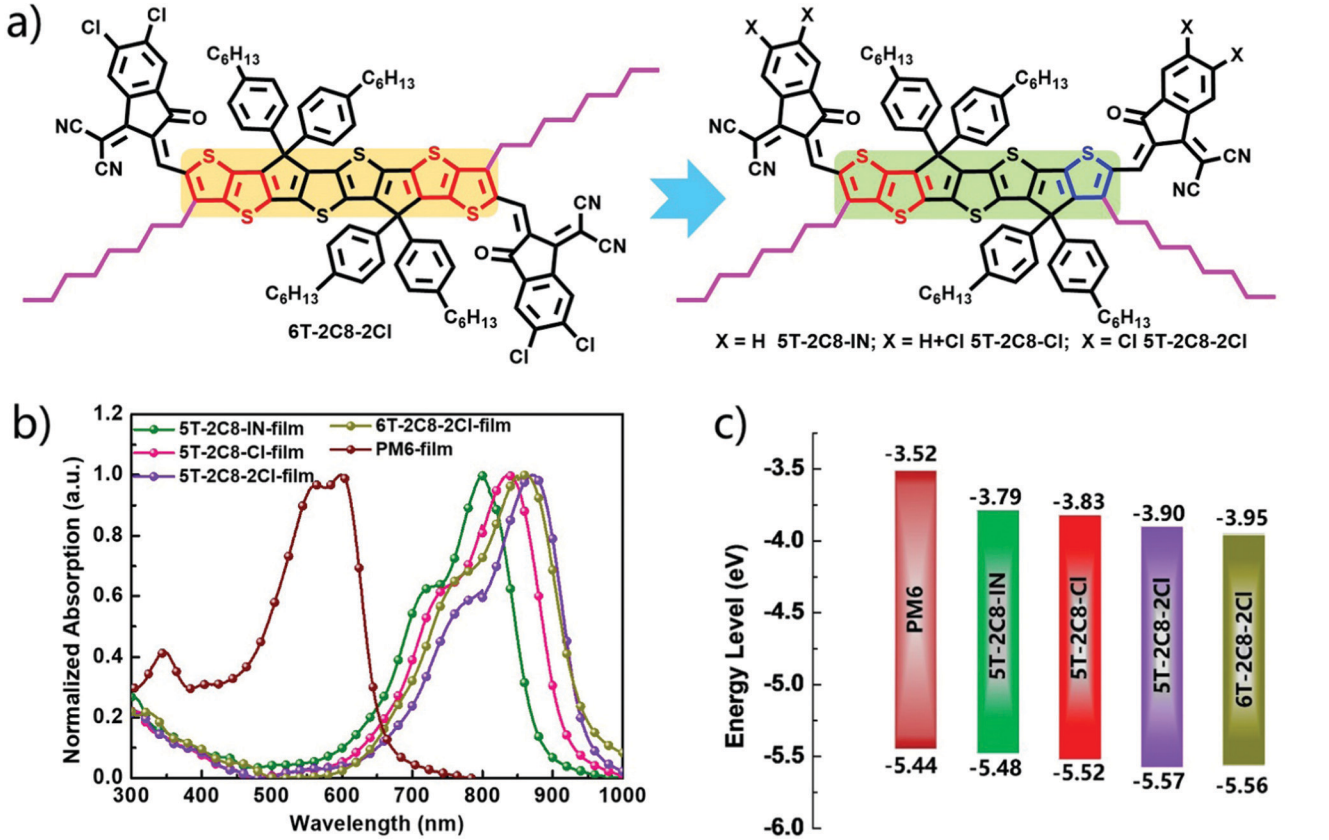

Fig. 1 (a) Chemical structures of **6T-2C8-2Cl**, **5T-2C8-IN**, **5T-2C8-Cl** and **5T-2C8-2Cl**, (b) normalized UV-vis-NIR absorption spectra of PM6, **5T-2C8-IN**, **5T-2C8-Cl**, **5T-2C8-2Cl** and **6T-2C8-2Cl** neat films, and (c) energy level diagram of PM6, **5T-2C8-IN**, **5T-2C8-Cl**, **5T-2C8-2Cl** and **6T-2C8-2Cl**.

Table 1 The optical and electrochemical properties of **5T-2C8-IN**, **5T-2C8-Cl**, **5T-2C8-2Cl** and **6T-2C8-2Cl**

Acceptors	λ_{max}^{CF} (nm)	λ_{max}^{film} (nm)	ε ($\times 10^5$ M^{-1} cm^{-1})	λ_{edge}^{film} (nm)	HOMO (eV)	LUMO (eV)	E_g^{CV} (eV)	E_g^{opt} (eV)
5T-2C8-IN	770	801	2.44	895	−5.48	−3.79	1.69	1.39
5T-2C8-Cl	785	838	2.61	939	−5.52	−3.83	1.69	1.32
5T-2C8-2Cl	796	871	2.64	960	−5.57	−3.90	1.67	1.29
6T-2C8-2Cl	809	860	2.41	959	−5.56	−3.95	1.61	1.29

planar conjugations for their backbones, which is beneficial to achieve effective intermolecular π–π stacking and good charge transport channels. The configuration change of asymmetric **5T-2C8-2Cl** shows a "C" shaped skeleton, which plays an important role in facilitating the intermolecular π–π stacking.[42,43] In contrast, **6T-2C8-2Cl** exhibits a "Z" shaped configuration as depicted in Fig. S3 (ESI†).[44,45]

The energy levels of the three asymmetric NFAs together with **6T-2C8-2Cl** for comparison were measured by cyclic voltammetry (Fig. S3b, ESI†) in acetonitrile on solid films. As shown in Fig. 1c, the HOMOs and LUMOs were estimated to be −5.48/−3.79, −5.52/−3.83, −3.57/−3.90 and −5.56/−3.95 eV for **5T-2C8-IN**, **5T-2C8-Cl**, **5T-2C8-2Cl** and **6T-2C8-2Cl**, respectively. These results indicate that the introduction of chlorine at the end groups indeed downshifts the energy levels, especially the LUMOs. Furthermore, the asymmetric acceptor **5T-2C8-2Cl** demonstrated a relatively higher LUMO energy level compared to that of the control symmetric **6T-2C8-2Cl**, which is expected to offer an improved V_{oc} value for **5T-2C8-2Cl** based OSCs (Table 1).

2.3. Photovoltaic performances

To evaluate the photovoltaic properties of **5T-2C8-IN**, **5T-2C8-Cl** and **5T-2C8-2Cl**, OSCs with an inverted device structure of ITO/ZnO/PFN-Br/PM6:NFA/MoO_x/Ag were fabricated, in which the wide band gap polymer PM6 was selected as the donor material owing to the matched energy levels and complementary absorptions with these acceptors. The device optimization process under different conditions is summarized in Tables S1–S9 (ESI†), including the donor/acceptor weight ratio (m%), the amount of additive (1,8-diiodine octane, DIO, vol%), thermal annealing (TA) conditions, *etc.* After systematic optimization, chlorobenzene was selected as the solvent, the optimized amount of DIO is 0.6% and the best TA temperature is 140 °C

Table 2 The optimized photovoltaic parameters of **5T-2C8-IN**, **5T-2C8-Cl**, **5T-2C8-2Cl** and **6T-2C8-2Cl** based devices under the illumination of AM 1.5G (100 mW cm^{-2})

Devices	V_{oc} (V)	FF	J_{sc} (mA cm^{-2})	J_{sc}^{EQE} (mA cm^{-2})	PCE[a] (%)
PM6:5T-2C8-IN	0.965 (0.963 ± 0.03)	0.51 (0.50 ± 0.01)	10.24 (10.12 ± 0.21)	9.95	5.04 (4.82 ± 0.30)
PM6:5T-2C8-Cl	0.864 (0.861 ± 0.03)	0.64 (0.64 ± 0.01)	20.86 (20.62 ± 0.26)	19.91	11.53 (11.22 ± 0.23)
PM6:5T-2C8-2Cl	0.802 (0.800 ± 0.03)	0.65 (0.64 ± 0.02)	24.97 (24.80 ± 0.20)	23.77	13.02 (12.87 ± 0.23)
PM6:6T-2C8-2Cl	0.785 (0.782 ± 0.04)	0.65 (0.64 ± 0.01)	24.40 (24.22 ± 0.17)	23.80	12.43 (12.25 ± 0.18)[b]

[a] The PCE value was calculated from 20 devices. [b] The data were cited from ref. 50.

for the devices based on these four acceptors. The optimized photovoltaic parameters are summarized in Table 2 and the corresponding current density–voltage (*J*–*V*) curves are shown in Fig. 2a. As shown in Table 2, **5T-2C8-IN**, **5T-2C8-Cl** and **5T-2C8-2Cl** based devices showed the best PCEs of 5.04%, 11.53% and 13.02%, respectively. The V_{oc} of the three optimized devices decreased with the increasing number of chlorine atoms on the end groups owing to the down shifted LUMOs, while the J_{sc} was gradually enhanced due to the red-shifted and broadened absorption range. It is worth noting that the **5T-2C8-2Cl** based device demonstrated an impressively higher PCE of 13.02% with the simultaneously improved V_{oc} of 0.802 V and a J_{sc} of 24.97 mA cm^{-2} compared with the acceptor **6T-2C8-2Cl** based device with a PCE of 12.43%, a V_{oc} of 0.785 V and a J_{sc} of 24.40 mA cm^{-2}. In addition, the 5T-2C8-2C based device with a conventional structure has also been fabricated and a comparable PCE of 12.20% has been achieved (Table S11, ESI†).

The external quantum efficiency (EQE) curves of the optimized devices are shown in Fig. 3b. For the three asymmetric 5T based devices, the EQE response was significantly enhanced after chlorination of the end groups and extended to around 960 nm for the **5T-2C8-2Cl** based device. Compared with the **5T-2C8-2Cl device**, the **6T-2C8-2Cl** based device showed a relatively lower EQE response but a slightly broader EQE range, which is consistent with the blend film absorptions (Fig. S2, ESI†). The integrated J_{sc} values of the four optimized devices are in good agreement with the corresponding J_{sc} values measured from *J*–*V* curves (error of less than 5%).

2.4. Carrier dynamics study

For further evaluating the exciton dissociation and charge collection properties of these four NFA based solar cells, the photocurrent density (J_{ph}) *versus* applied voltage (V_{eff}) was measured. Herein, $J_{ph} = J_L - J_D$, where J_L and J_D are the current

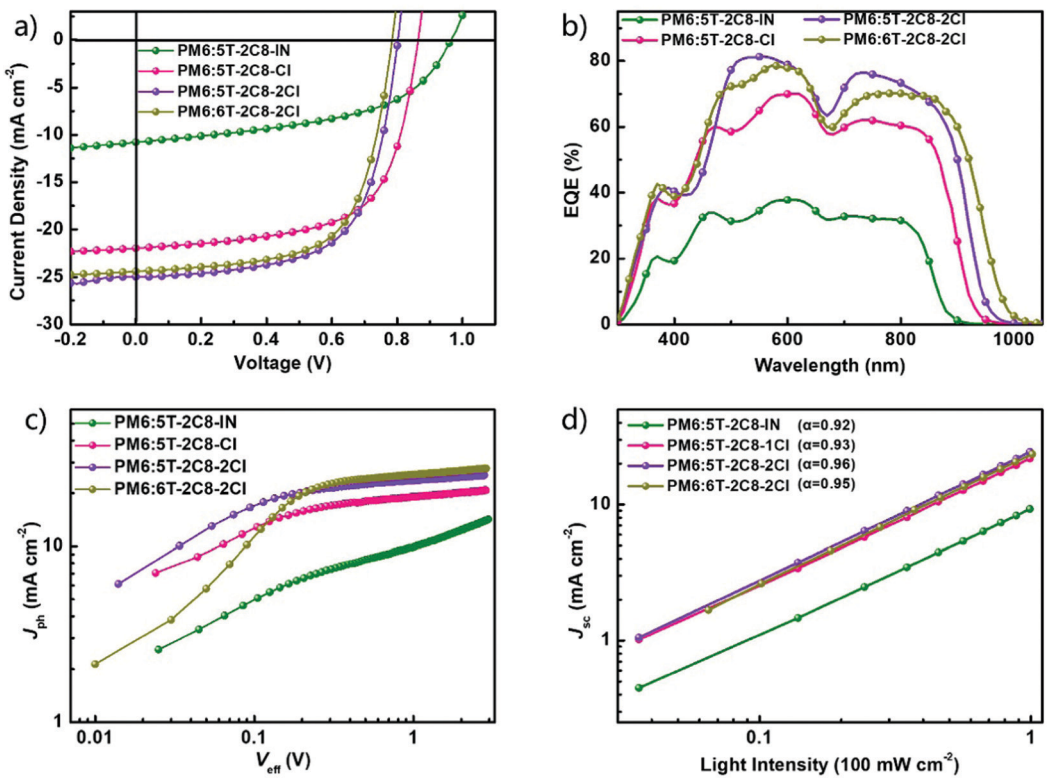

Fig. 2 (a) *J*–*V* curves of PM6:**5T-2C8-IN**/**5T-2C8-1Cl**/**5T-2C8-2Cl** and PM6:**6T-2C8-2Cl** based devices under one sun illumination (AM 1.5G 100 mW cm^{-2}). (b) EQE spectra of the corresponding devices. (c) J_{ph} *versus* V_{eff} and (d) light-intensity (*P*) dependence of J_{sc} measurement of the devices.

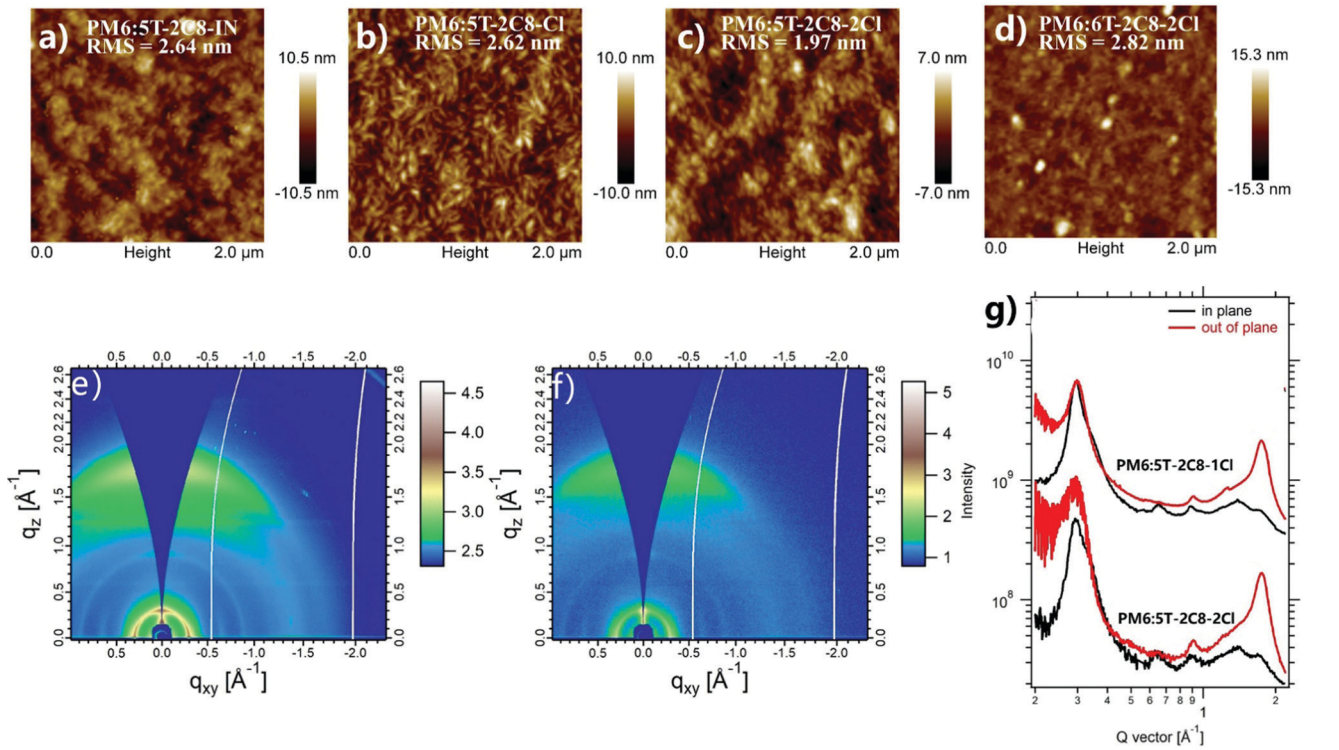

Fig. 3 AFM images of the blend films based on **5T-2C8-IN** (a), **5T-2C8-1Cl**, (b) **5T-2C8-2Cl,** (c) and **6T-2C8-2Cl** (d), the 2D GIWAXS patterns based on PM6:**5T-2C8-1Cl** (e) and PM6:**5T-2C8-2Cl** (f) and the corresponding line-cut profiles (g).

densities under light illumination and in the dark, respectively, and V_{eff} is calculated as $V_{eff} = V_o - V_a$, in which V_a is the applied voltage and V_o is the voltage when $J_{ph} = 0$.[46,47] As shown in Fig. 3c, these four devices all reach saturation (J_{sat}) when V_{eff} reaches ~1.5 V, illustrating that at a higher voltage, the charge recombination is minimal for these devices. Then the value of J_{ph}/J_{sat} representing the charge dissociation and the collection probability ($P(E, T)$) was studied to investigate the charge carrier dynamics. The devices based on **5T-2C8-IN**, **5T-2C8-Cl**, **5T-2C8-2Cl** and **6T-2C8-2Cl** gave J_{ph}/J_{sat} values of 69%, 90%, 92% and 91% under short-circuit density conditions and 44%, 74%, 78% and 76%, under maximal power output conditions, respectively. The **5T-2C8-2Cl** based device showed the highest J_{ph}/J_{sat} values under short-circuit current density and maximal power output conditions, demonstrating the best exciton dissociation and efficient charge collection efficiency in these devices.[48]

The light-intensity dependence (P) of J_{sc} was measured to further study the charge recombination behaviour of the corresponding devices (Fig. 2d). The light intensity (P) and J_{sc} abided the power-law equation of $J_{sc} \propto P^{\alpha}$, where the exponent α represents the bimolecular recommendation extent. The device with an α value ~1 indicates the weaker degree of bimolecular recombination.[47] The α values were 0.92, 0.93, 0.96 and 0.95 for **5T-2C8-IN**, **5T-2C8-Cl**, **5T-2C8-2Cl** and **6T-2C8-2Cl** based devices, respectively. These results demonstrate that the **5T-2C8-2Cl** based device exhibited least bimolecular recombination among the devices based on these four acceptors.

The charge mobilities were measured using the space charge limit current (SCLC) method with the electron and hole only devices (Fig. S4, ESI†). The electron and hole mobilities of PM6:**5T-2C8-2Cl** and PM6:**6T-2C8-2Cl** based devices were calculated to be $6.05 \times 10^{-5}/3.99 \times 10^{-4}$ and $2.85 \times 10^{-5}/5.08 \times 10^{-5}$ cm^{-2} V^{-1} s^{-1}, respectively, which are higher than those of PM6:**5T-2C8-IN** ($9.13 \times 10^{-6}/3.38 \times 10^{-5}$ cm^{-2} V^{-1} s^{-1}) and PM6:**5T-2C8-Cl** ($2.77 \times 10^{-5}/2.11 \times 10^{-4}$ cm^{-2} V^{-1} s^{-1}). The mobility values as well as the exciton dissociation and bimolecular recombination results indicate that the asymmetric molecular backbone and side chain modulation generate favourable effects on the device working process and is a promising strategy for the active layer material design to achieve high-efficiency OSCs.

2.5. Morphology characterization

Atomic force microscopy (AFM) was used to investigate the blend films of the three asymmetric acceptors with PM6. As shown in Fig. 3a–d and the corresponding phase images in Fig. S5 (ESI†), PM6:**5T-2C8-IN** and PM6:**5T-2C8-Cl** blend films show relatively larger aggregates with root-mean-square (RMS) values of 2.64 and 2.62 nm, respectively, which is similar to that of the PM6:**6T-2C8-2Cl** (2.82 nm) blend film.[49] Whereas, a nano-fibrillar network was observed in the **5T-2C8-2Cl** blend film with a RMS surface roughness of 1.97 nm. Furthermore, the PM6:**5T-2C8-2Cl** based blend film exhibits a clear nanoscale network with a small root-mean-square (RMS) surface roughness of 1.97 nm, which indicates a well matched compatibility

between PM6 and **5T-2C8-2Cl**. Furthermore, grazing incidence wide angle X-ray scattering (GIWAXS) was used to investigate the molecular packing properties of **5T-2C8-Cl** and **5T-2C8-2Cl** based blend films. As shown in Fig. 3f, the **5T-2C8-Cl** and **5T-2C8-2Cl** based blend films adopt a face-on orientation with an intense π–π diffraction peak in the out-of-plane (OOP) direction and a lamellar diffraction peak in the in-plane (IP) direction. The **5T-2C8-2Cl** blend film shows a clear π–π stacking diffraction peak (010) at 1.75 $Å^{-1}$, with a π–π *d*-spacing distance of 3.59 Å in the OOP direction, which is more compact than that of the **5T-2C8-Cl** blend film with π–π *d*-spacing distance of 3.61 Å (OOP diffraction peak (010) at 1.74 $Å^{-1}$). In contrast, the PM6:**6T-2C8-2Cl** blend film exhibits an OOP diffraction peak at 1.82 $Å^{-1}$ with a π–π *d*-spacing distance of 3.45 Å.[12,50] Despite the slightly larger π–π distance in the PM6:**5T-2C8-2Cl** blend film compared with that of PM6:**6T-2C8-2Cl** blend film, the crystal coherence length (CCL) for the PM6:**5T-2C8-2Cl** blend film estimated from Scherrer's equation[51] (CCL = $2\pi k$/fwhm) by Gaussian fitting with the full-width at half-maximum (fwhm) is 24.1 Å, which is larger than that of the **6T-2C8-2Cl** based blend film (CCL of 18.8 Å).[50] This demonstrates the enhanced crystallinity in the blend film of PM6:**5T-2C8-2Cl**, facilitating the charge transport in the photovoltaic device. Compared with the "Z" type molecular skeleton of the symmetric acceptor **6T-2C8-2Cl**, the "C" type configuration of the asymmetric acceptor **5T-2C8-2Cl** should be the intrinsic factor that determines the packing difference of the two acceptor based blend films. The results also demonstrate that careful modulation of the molecular skeleton should be one of the effective ways for the morphology control of the active layer.

3. Conclusions

In summary, following the strategy of fine-tuning the molecular configuration in combination with the side chain modulation to simultaneously improve the V_{oc} and J_{sc}, three acceptors with asymmetric molecular skeletons and octyl side chains at the terminal position of the molecular backbones, **5T-2C8-IN**, **5T-2C8-Cl** and **5T-2C8-2Cl**, have been designed and synthesized. Among them, the **5T-2C8-2Cl** based solar cell demonstrated the best PCE of 13.02% with a simultaneously improved J_{sc} of 24.97 mA cm^{-2} and a V_{oc} of 0.794 V, compared with the control symmetric acceptor **6T-2C8-2Cl** based device with a PCE of 12.43%, a J_{sc} of 24.40 mA cm^{-2} and a V_{oc} of 0.785 V. The results indicate that the J_{sc} and V_{oc} can be simultaneously enhanced through careful molecular structural regulation. Considering the large variety of organic materials and current promising results in the OSC field, it is believed that high efficiency active layer materials can be rationally designed to encounter the issue of J_{sc} and V_{oc} trade-off and obtain higher device performance.

Conflicts of interest

There are no conflicts to declare.

Acknowledgements

This work was supported by the Natural Science Foundation Research Project of Shaanxi Province (No. 2021JQ-595), the Scientific Research Program Funded by Shaanxi Provincial Education Department (No. 20JK0841), the NSFC (21935007, 21704082) and the Key Scientific and Technological Innovation Team Project of Shaanxi Province (2020TD-002). X-ray data were acquired at beamlines 7.3.3 at the Advanced Light Source, which is supported by the Director, Office of Science, Office of Basic Energy Sciences, the U.S. Department of Energy under Contract No. DE-AC02-05CH11231. The authors thank Chenhui Zhu at beamline 7.3.3 for assistance with data acquisition.

Notes and references

1 X. Wan, M. Zhang and Y. Chen, *Chem. Soc. Rev.*, 2020, **49**, 2828–2842.
2 C. Yan, S. Barlow, Z. Wang, H. Yan, A. K. Y. Jen, S. R. Marder and X. Zhan, *Nat. Rev. Mater.*, 2018, **3**, 18003.
3 G. Zhang, J. Zhao, P. C. Y. Chow, K. Jiang, J. Zhang, Z. Zhu, J. Zhang, F. Huang and H. Yan, *Chem. Rev.*, 2018, **118**, 3447–3507.
4 L. Meng, Y. Zhang, X. Wan, C. Li, X. Zhang, Y. Wang, X. Ke, Z. Xiao, L. Ding, R. Xia, H.-L. Yip, Y. Cao and Y. Chens, *Science*, 2018, **361**, 1094–1098.
5 C. Li, J. Zhou, J. Song, J. Xu, H. Zhang, X. Zhang, J. Guo, L. Zhu, D. Wei, G. Han, J. Min, Y. Zhang, Z. Xie, Y. Yi, H. Yan, F. Gao, F. Liu and Y. Sun, *Nat. Energy*, 2021, **6**, 605–613.
6 Y. Lin, A. Magomedov, Y. Firdaus, D. Kaltsas, A. El-Labban, H. Faber, D. R. Naphade, E. Yengel, X. Zheng, E. Yarali, N. Chaturvedi, K. Loganathan, D. Gkeka, S. H. AlShammari, O. M. Bakr, F. Laquai, L. Tsetseris, V. Getautis and T. D. Anthopoulos, *ChemSusChem*, 2021, **14**, 3569–3578.
7 G. Liu, R. Xia, Q. Huang, K. Zhang, Z. Hu, T. Jia, X. Liu, H. L. Yip and F. Huang, *Adv. Funct. Mater.*, 2021, 2103283.
8 Y. Xu, Y. Cui, H. Yao, T. Zhang, J. Zhang, L. Ma, J. Wang, Z. Wei and J. Hou, *Adv. Mater.*, 2021, 2101090.
9 P. Bi, S. Zhang, Z. Chen, Y. Xu, Y. Cui, T. Zhang, J. Ren, J. Qin, L. Hong, X. Hao and J. Hou, *Joule*, 2021, **5**, 2408–2419.
10 J. Wang, Z. Zheng, Y. Zu, Y. Wang, X. Liu, S. Zhang, M. Zhang and J. Hou, *Adv. Mater.*, 2021, 2102787.
11 B. Fan, X. Du, F. Liu, W. Zhong, L. Ying, R. Xie, X. Tang, K. An, J. Xin, N. Li, W. Ma, C. J. Brabec, F. Huang and Y. Cao, *Nat. Energy*, 2018, **3**, 1051–1058.
12 H. H. Gao, Y. Sun, Y. Cai, X. Wan, L. Meng, X. Ke, S. Li, Y. Zhang, R. Xia, N. Zheng, Z. Xie, C. Li, M. Zhang, H. L. Yip, Y. Cao and Y. Chen, *Adv. Energy Mater.*, 2019, **9**, 1901024.
13 Y. Qin, Y. Chen, Y. Cui, S. Zhang, H. Yao, J. Huang, W. Li, Z. Zheng and J. Hou, *Adv. Mater.*, 2017, **29**, 1606340.
14 W. Zhao, S. Li, H. Yao, S. Zhang, Y. Zhang, B. Yang and J. Hou, *J. Am. Chem. Soc.*, 2017, **139**, 7148–7151.
15 G. Li, W.-H. Chang and Y. Yang, *Nat. Rev. Mater.*, 2017, **2**, 17043.

16 P. Cheng, G. Li, X. Zhan and Y. Yang, *Nat. Photonics*, 2018, **12**, 131–142.
17 J. Hou, O. Inganas, R. H. Friend and F. Gao, *Nat. Mater.*, 2018, **17**, 119–128.
18 Y. Lin, J. Wang, Z. G. Zhang, H. Bai, Y. Li, D. Zhu and X. Zhan, *Adv. Mater.*, 2015, **27**, 1170–1174.
19 J. Yuan, Y. Zhang, L. Zhou, G. Zhang, H.-L. Yip, T.-K. Lau, X. Lu, C. Zhu, H. Peng, P. A. Johnson, M. Leclerc, Y. Cao, J. Ulanski, Y. Li and Y. Zou, *Joule*, 2019, **3**, 1140–1151.
20 S. Li, L. Zhan, N. Yao, X. Xia, Z. Chen, W. Yang, C. He, L. Zuo, M. Shi, H. Zhu, X. Lu, F. Zhang and H. Chen, *Nat. Commun.*, 2021, **12**, 4627.
21 Z. Bi, K. Chen, L. Gou, Y. Guo, X. Zhou, H. B. Naveed, J. Wang, Q. Zhu, J. Yuan, C. Zhao, K. Zhou, S. Chandrabose, Z. Tang, Y. Yi, J. M. Hodgkiss, L. Zhang and W. Ma, *J. Mater. Chem. A*, 2021, **9**, 16733–16742.
22 M. Chang, Y. Zhang, B.-S. Lu, D. Sui, F. Wang, J. Wang, Y. Yang and B. Kan, *Chem. Eng. J.*, 2022, **427**, 131473.
23 T. Shan, K. Ding, L. Yu, X. Wang, Y. Zhang, X. Zheng, C. C. Chen, Q. Peng and H. Zhong, *Adv. Funct. Mater.*, 2021, **31**, 2100750.
24 K. Jiang, Q. Wei, J. Y. L. Lai, Z. Peng, H. K. Kim, J. Yuan, L. Ye, H. Ade, Y. Zou and H. Yan, *Joule*, 2019, **3**, 3020–3033.
25 X. Zhang, C. Li, L. Qin, H. Chen, J. Yu, Y. Wei, X. Liu, J. Zhang, Z. Wei, F. Gao, Q. Peng and H. Huang, *Angew. Chem., Int. Ed.*, 2021, **60**, 17720–17725.
26 J. Subbiah, C. J. Lee, V. D. Mitchell and D. J. Jones, *ACS Appl. Mater. Interfaces*, 2020, **13**, 1086–1093.
27 J. Subbiah, B. Purushothaman, M. Chen, T. Qin, M. Gao, D. Vak, F. H. Scholes, X. Chen, S. E. Watkins, G. J. Wilson, A. B. Holmes, W. W. Wong and D. J. Jones, *Adv. Mater.*, 2015, **27**, 702–705.
28 S. Li, L. Ye, W. Zhao, S. Zhang, S. Mukherjee, H. Ade and J. Hou, *Adv. Mater.*, 2016, **28**, 9423–9429.
29 H. Lu, H. Jin, H. Huang, W. Liu, Z. Tang, J. Zhang and Z. Bo, *Adv. Funct. Mater.*, 2021, 2103445.
30 H. Yu, S. Luo, R. Sun, I. Angunawela, Z. Qi, Z. Peng, W. Zhou, H. Han, R. Wei, M. Pan, A. M. H. Cheung, D. Zhao, J. Zhang, H. Ade, J. Min and H. Yan, *Adv. Funct. Mater.*, 2021, **31**, 2100791.
31 C. Tang, X. Ma, J. Y. Wang, X. Zhang, R. Liao, Y. Ma, P. Wang, P. Wang, T. Wang, F. Zhang and Q. Zheng, *Angew. Chem., Int. Ed.*, 2021, **60**, 2–12.
32 B. Kan, H. Feng, X. Wan, F. Liu, X. Ke, Y. Wang, Y. Wang, H. Zhang, C. Li, J. Hou and Y. Chen, *J. Am. Chem. Soc.*, 2017, **139**, 4929–4934.
33 N. Qiu, H. Zhang, X. Wan, C. Li, X. Ke, H. Feng, B. Kan, H. Zhang, Q. Zhang, Y. Lu and Y. Chen, *Adv. Mater.*, 2017, **29**, 1604964.
34 H. Feng, Y. Q. Q. Yi, X. Ke, J. Yan, Y. Zhang, X. Wan, C. Li, N. Zheng, Z. Xie and Y. Chen, *Adv. Energy Mater.*, 2019, **9**, 1803541.
35 Z. Wang, R. Wang, Y. Mi, K. Lu, Y. Liu, C. Yang, J. Zhang, X. Liu, Y. Wang, Z. Shuai and Z. Wei, *Chem. Mater.*, 2021, **33**, 4578–4585.
36 C. Li, H. Fu, T. Xia and Y. Sun, *Adv. Energy Mater.*, 2019, **9**, 1900999.
37 Y. Chen, R. Ma, T. Liu, Y. Xiao, H. K. Kim, J. Zhang, C. Ma, H. Sun, F. Bai, X. Guo, K. S. Wong, X. Lu and H. Yan, *Adv. Energy Mater.*, 2021, **11**, 2003777.
38 D. Hu, Q. Yang, Y. Zheng, H. Tang, S. Chung, R. Singh, J. Lv, J. Fu, Z. Kan, B. Qin, Q. Chen, Z. Liao, H. Chen, Z. Xiao, K. Sun and S. Lu, *Adv. Sci.*, 2021, **8**, 2004262.
39 W. Gao, H. Fu, Y. Li, F. Lin, R. Sun, Z. Wu, X. Wu, C. Zhong, J. Min, J. Luo, H. Y. Woo, Z. Zhu and A. K. Y. Jen, *Adv. Energy Mater.*, 2020, **11**, 2003177.
40 Q. Zhu, D. Liu, Z. Lu, C. Gu, K. Zhang, X. Bao, Q. Li and R. Yang, *J. Mater. Chem. A*, 2019, **7**, 4823–4828.
41 S. Li, L. Zhan, Y. Jin, G. Zhou, T. K. Lau, R. Qin, M. Shi, C. Z. Li, H. Zhu, X. Lu, F. Zhang and H. Chen, *Adv. Mater.*, 2020, **32**, 2001160.
42 N. Zarrabi, O. J. Sandberg, S. Zeiske, W. Li, D. B. Riley, P. Meredith and A. Armin, *Nat. Commun.*, 2020, **11**, 5567.
43 G. Zhang, X. K. Chen, J. Xiao, P. C. Y. Chow, M. Ren, G. Kupgan, X. Jiao, C. C. S. Chan, X. Du, R. Xia, Z. Chen, J. Yuan, Y. Zhang, S. Zhang, Y. Liu, Y. Zou, H. Yan, K. S. Wong, V. Coropceanu, N. Li, C. J. Brabec, J. L. Bredas, H. L. Yip and Y. Cao, *Nat. Commun.*, 2020, **11**, 3943.
44 Z. Zhang, J. Yu, X. Yin, Z. Hu, Y. Jiang, J. Sun, J. Zhou, F. Zhang, T. P. Russell, F. Liu and W. Tang, *Adv. Funct. Mater.*, 2018, **28**, 1705095.
45 D. Liu, L. Yang, Y. Wu, X. Wang, Y. Zeng, G. Han, H. Yao, S. Li, S. Zhang, Y. Zhang, Y. Yi, C. He, W. Ma and J. Hou, *Chem. Mater.*, 2018, **30**, 619.
46 L. Yang, X. Song, J. Yu, H. Wang, Z. Zhang, R. Geng, J. Cao, D. Baran and W. Tang, *J. Mater. Chem. A*, 2019, **7**, 22279–22286.
47 P. W. M. Blom, V. D. Mihailetchi, L. J. A. Koster and D. E. Markov, *Adv. Mater.*, 2007, **19**, 1551–1566.
48 C. M. Proctor, M. Kuik and T.-Q. Nguyen, *Prog. Polym. Sci.*, 2013, **38**, 1941–1960.
49 Z.-G. Zhang, B. Qi, Z. Jin, D. Chi, Z. Qi, Y. Li and J. Wang, *Energy Environ. Sci.*, 2014, **7**, 1966–1973.
50 Y. Sun, H.-H. Gao, S. Wu, L. Meng, X. Wan, M. Li, Z. Ma, Z. Guo, S. Li, H. Zhang, C. Li and Y. Chen, *Sci. China: Chem.*, 2021, **64**, 608–615.
51 D.-M. Smilgies, *J. Appl. Crystallogr.*, 2013, **46**, 286.

